

A Colliding-Wind Model for the Wolf–Rayet System HD 152270 (WR 79)¹

S. LÜHRS

Astronomisches Institut, Westfälische Wilhelms-Universität, Wilhelm-Klemm-Str. 10, D-48149 Münster, F.R. Germany
 Electronic mail: 100327.2626@compuserve.com

Received 1996 September 4; accepted 1997 February 12

ABSTRACT. New orbital elements for the binary system HD 152270 (WC7+O6) are derived from high-resolution observations and literature data, obtained between 1944 and 1989. Variations in position and structure of the peak profile, overlying the flat-topped C III 569.59 nm line, are used to derive a colliding-wind model (cone model) for the system. The model is used to construct synthetic line profiles which are compared with the observed profiles.

1. INTRODUCTION

Earlier investigations of HD 152270=WR 79 yield the following results: WR 79 is a double-lined spectroscopic binary with the components WC7+O5-8 (Smith et al. 1990).² The magnitude and color index in a narrow-band system which emulates the Johnson system, while avoiding the inclusion of strong WR emission lines, are given as $v=6.95$ and $b-v=0.01$. The distance $d=2.00$ kpc and absolute magnitude $M_v=-6.0$ are based on the membership of WR 79 in the open star cluster NGC 6231 (van der Hucht et al. 1988). The orbital period was determined by Struve (1944), Seggewiß (1974) and St.-Louis et al. (1987). The results range from $P=8.82$ d (Struve) to $P=8.893$ d, (adopted by Seggewiß from his derived value $P=8.89251$, errors not given). The inclination angle of the orbit was derived from polarization studies to $i=44:8 \pm 5:0$ (St.-Louis et al. 1987) and from a model to $i=35^\circ$ (Neutsch et al. 1979). The radial-velocity amplitudes are $K_1=51$ km s⁻¹ (O6 star), $K_2=142$ km s⁻¹ (WR-star), and $\gamma=-27.2$ km s⁻¹ (Seggewiß 1974). Mass estimates range from $M_{WR}=5M_\odot$ (St.-Louis et al. 1987) to $M_{WR}\approx 11M_\odot$ (Neutsch et al. 1979).

The most striking feature in the optical spectrum of WR 79 is the *peak profile* overlying the flat-topped C III line at 569.59 nm. The peak profile is defined as the additional light on the flat C III profile, measured from the rise of the superimposed blue peak to the decline of the red peak. Seven spectra taken at different phases show that the total (=base + peak) profile changes its shape and position systematically as a function of orbital phase of the binary system. The pattern at a given phase shows a tendency to repeat, even after more than 160 cycles of the system, as shown in Fig. 1. Smaller variations may be attributed to additional C III emission from turbulent clumps (as also seen in other WC stars,

Moffat et al. 1994). In the following, the main pattern will be used to derive a model for WR 79.

The C III line had attracted attention through its variable substructures, first described by Seggewiß (1974) as “moving emission peaks superimposed on the top of the emission line . . . [which] may be attributed to gas streams in the stellar envelope.” Neutsch (1979) and Neutsch et al. (1979, 1981) derived a quantitative model assuming an *emission-free* region in the WR envelope, caused by perturbations due to the O star, to account for “the *depression* on the line top.” In the present communication it is shown that *emission peaks* are well reproduced by a colliding wind model, although it is left to further investigations to improve some of the fits, both by forthcoming observations as well as quantitative explanations of the deficiencies using a more detailed model.

2. OBSERVATIONS

The C III 569.59 nm line of WR 79 was observed at ESO-La Silla with the ESO 1.4-m Coudé Auxiliary Telescope (CAT) plus Coudé Echelle Spectrometer (CES) and the ESO 1.52-m telescope plus B&C Cassegrain spectrograph (see Table 1). The extreme linewidth of about 9 nm could not be covered by a single setting of the CES. In 1985, using a Reticon, the line was covered by three to four exposures, each with observing times of 30–50 min. Substructures of widths more than 0.2 nm show no significant changes during this time. The CCD spectra of 1989 consist of two overlapping exposures. No significant changes occur in the CCD spectra during the exposure time of the order of one minute.

Three UV spectra of WR 79, obtained with the *IUE* satellite in high-resolution mode, show that the C III 190.9 nm line has essentially the same appearance as the optical line, including the superimposed peaks (Groote, private communication). The UV data are, however, too scarce for an independent derivation of the model.

WR 79 ranges among the moderate WR X-ray sources (Pollock et al. 1995). Data covering a sufficiently large part of the orbital cycle are needed to test the X-ray variability

¹Based on observations collected at the European Southern Observatory, La Silla, Chile.

²For the secondary, Smith et al. give a spectral type O5-8; Seggewiß (1974) derives O5 from MK spectral classification; Abbott et al. (1986) list both O5 and O6. We will adopt the spectral type O6V, which is in good agreement with the mass of the O star derived in this paper.

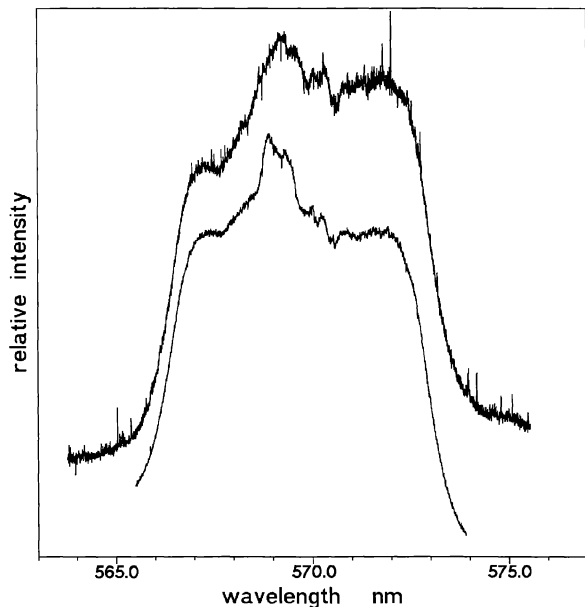


FIG. 1—The upper profile was observed at the Coriolis corrected phase angle $\varphi - \theta = 307^\circ$ in 1985, the lower profile at $305^\circ.7$ in 1989. The two lines are shown at almost equal phase with a time difference of more than 160 periods. The similarity extends from the major peak profile to several smaller features. The stability of the large features is explained by the model derived in the following sections.

suggested by the geometrical model proposed in the present paper.

3. ORBITAL PERIOD OF WR 79

3.1 Data

The radial velocities of the WR component of the system are determined from the positions of the C III 569.59 nm emission-line center. Two versions of Pogson's bisecting method are used.

Method (I) emulates Pogson's original method for determining the minimum and maximum times of variable stars (Hoffmeister et al. 1990): A number of lines parallel to the spectral continuum and located at various intensity levels within the emission feature are bisected. A straight line is fitted to the centers. The fitted line is extrapolated to the continuum level, where it marks the central wavelength of the total emission feature.

This method was applied to the low-resolution spectra taken in 1988 and to the high-resolution spectra of 1989 (Fig. 2). The latter are obtained from exposures of two overlapping parts of the line taken within a short time interval. No reference continuum is available and we assume that the con-

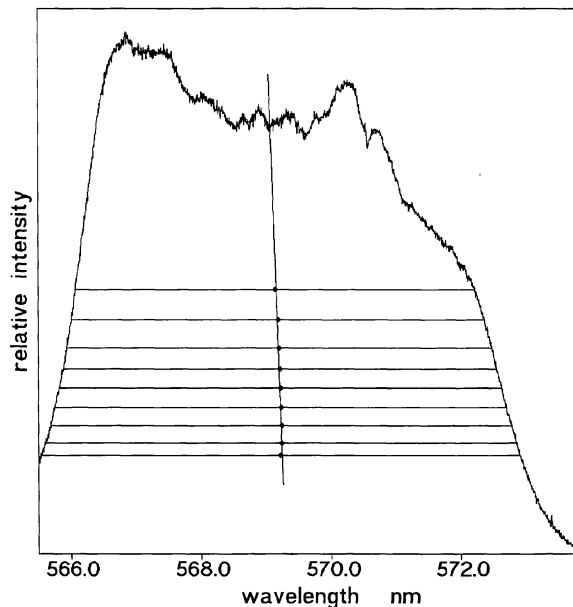


FIG. 2—Profile of the C III line on HJD 2 447 779.498. Pogson's method (I) is applied under the assumption that the continuum is flat (see text).

tinuum is flat, although this may lead to errors. The radial velocities from the spectra of 1989 show, indeed, somewhat larger deviations from the mean RV curve than to the results from the other two series.

Method (II) is applied to the segmented high-resolution spectra of 1985 (Fig. 3). The continuum as well as the part of the flat top of the emission line which is adjacent to the downward slope are fitted by parallel horizontal lines. A third parallel is introduced midway between the pair of parallels. The latter intersects the red (or blue) slope of the emission line. The projections from both intersections onto the continuum define the total wavelength interval. Its bisection marks the center of the emission line. The continua red-

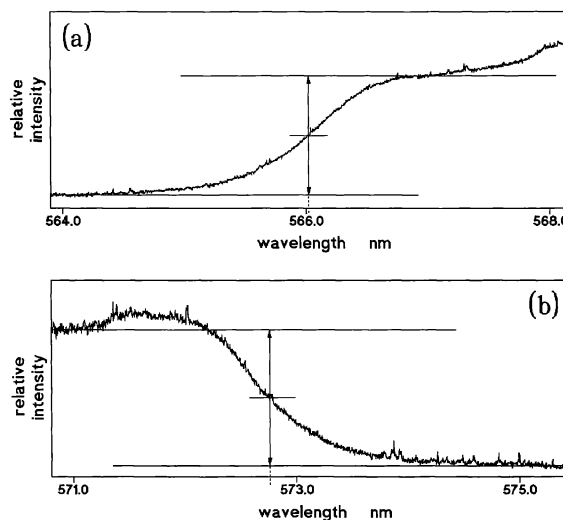


FIG. 3—The blue wing (a) and the red wing (b) of the C III line of WR 79 together with the adjacent continua and the adjacent parts of the emission plateau were taken on HJD 2 446 314.6. They are used by method (II) for the determination of the line center. For details see text.

TABLE 1
Observations of WR 79

Year	Telescope and Instrument	$\frac{\lambda}{\Delta\lambda}$
1985	1.4-m CAT + CES, Reticon	50,000
1988	1.5-m ESO + B&C, CCD	1000
1989	1.4-m CAT + CES, CCD	60,000

TABLE 2
Heliocentric Radial Velocities of the C III Line

1985		1988		1989	
HJD*	RV	HJD*	RV	HJD*	RV
309.577	+97.1	1211.845	-137.0	1778.493	-149.1
313.576	-139.1	1212.899	-114.0	1779.498	-216.1
314.586	-140.1	1214.896	+68.0	1783.587	-40.1
315.575	-58.8	1215.894	+103.0	1784.481	+29.1
316.588	+16.8	1216.902	+70.0	1785.472	-7.5
318.590	+47.1	1217.906	-151.0	1786.470	-69.0
319.567	-30.9	1787.474	-155.0
...	1788.481	-228.0

*Add 2446000 to the given date to obtain HJD.

ward and blueward of the line wings were determined interactively, as were the red and blue levels of the flat line top. The red and blue wings of the C III line were observed within time intervals of up to four hours. The resulting positional inaccuracies amount to at most 7% and do not affect the conclusions. The heliocentric radial velocities thus derived are listed in Table 2.

3.2 Determination of the Period

The data in Table 2, together with those of Struve (1944) and Seggewi β (1974), are used unweighted, in spite of their different quality, since no reliable quality criteria are available. The simplex algorithm is used for the nonlinear least squares fit to the data (Caceci and Cacheris 1984; Duerbeck et al. 1987); the period is the independent variable. The starting values for the period are varied within the interval 7.5 to 9.5 days. The stepsize of 0.01 days ensures that the fit finds the local minimum nearest to the starting value. The remaining parameters of the radial-velocity curve are optimized for this period. The formal errors of the parameters are calculated using the curvature of the χ^2 surface, assuming that the individual parameters are independent of each other. The choice between the two most likely periods, 8.237341 d \pm 0.000166 d and 8.891037 d \pm 0.000176 d, is made later in favor of the long period (see Sec. 8). The orbital data for the short and the long period are given in Table 3.

4. MOVING EMISSION PEAKS ON THE FLAT-TOPPED C III LINE

Two large emission peaks are superimposed on the plateau of the C III line (see, e.g., Fig. 2). Their widths lie roughly between 1 and 2 nm. At most orbital phases they are noticeably asymmetric, except near the Coriolis-corrected phase 180° (as is observed) and at phase 0 (as is expected). Over the orbital period, their positions shift along the plateau

TABLE 3
Orbital Elements for the Derived Periods

	Units	Short Period	Long Period
P	d	8.237341 \pm 0.000166	8.891037 \pm 0.000176
K_2	km s ⁻¹	128.1 \pm 10.3	132.6 \pm 10.8
γ	km s ⁻¹	-52.3 \pm 4.7	-55.0 \pm 4.7
t_0	HJD	2441161.109 \pm 0.107	2441160.689 \pm 0.107
σ_{RV}	km s ⁻¹	43.03	43.19

TABLE 4
Heliocentric Radial Velocities v of the Peaks on the C III Line at Different Epochs, v' Radial Velocities Referred to the Center of the WR Star, Using the Long Period

HJD*	v_{blue}	v_{red}	v'_{blue}	v'_{red}
1971				
1161.681	-1097.0	803.0	-1143.4	756.6
1162.563	-1304.0	433.5	-1281.4	456.1
1163.514	-1486.0	50.5	-1376.3	160.2
1164.530	-1316.0	328.0	-1140.4	503.6
1165.510	-1082.0	788.5	-899.1	971.4
1166.565	-683.5	1175.0	-558.1	1300.4
1167.524	-240.5	1291.5	-201.1	1330.9
1168.681	-356.5	1380.0	-408.2	1328.3
1169.535	-752.5	981.5	-830.0	904.0
1985				
6309.551	-1019.6	...	-1068.4	...
6309.602	...	862.2	...	816.5
6313.546	...	851.6	...	1030.9
6313.605	-933.3	...	-756.0	...
6314.586	-634.0	...	-517.6	...
6314.638	...	1051.8	...	1163.9
6315.550	...	1234.9	...	1263.6
6315.600	-349.5	...	-325.3	...
6316.588	-182.0	...	-233.5	...
6316.629	...	1127.9	...	1074.1
6318.522	-1153.1	...	-1197.0	...
6318.590	...	710.8	...	671.2
6319.479	-1401.0	...	-1367.9	...
6319.567	...	409.8	...	451.1
1988				
7211.847	-1008.5	861.5	-841.9	1028.1
7212.899	-536.5	1157.5	-447.8	1246.2
7214.896	-435.2	1107.8	-501.5	1041.5
7215.895	-761.1	1057.9	-833.2	985.8
7216.902	-1132.0	594.0	-1148.6	577.4
7217.905	-1374.0	172.0	-1300.6	245.4
1989				
7778.493	-1480.1	215.0	-1366.3	328.7
7779.498	-1447.1	319.9	-1270.1	496.9
7783.587	-383.1	1196.9	-433.4	1146.6
7784.481	-602.0	912.1	-679.5	834.5
7785.472	-1095.9	736.1	-1144.1	687.9
7786.470	-1369.8	319.2	-1339.5	349.5
7787.474	-1479.8	277.2	-1358.7	398.3
7788.481	-1391.7	363.3	-1211.6	543.4

*Add 2440000 to the given date to obtain HJD.

References—1971 — see Neutsch et al. (1979).

of the C III line. Some smaller emissions may be due to long-lived secondary processes (see Fig. 1). The changing positions of the peak maxima were measured. The corresponding heliocentric radial velocities v_{blue} and v_{red} are given in Table 4. With the orbital period P , the amplitude K_2 and the systemic velocity γ from Table 3, the measured radial velocities v_{blue} and v_{red} are reduced to the center of the WR star. The transformation is made for the long period given in Table 3. The heliocentric radial velocities v_{blue} , v_{red} and the radial velocities v'_{blue} , v'_{red} , referred to the center of the WR star, are listed in Table 4.

The radial velocities of the peaks are presented in Sec. 8

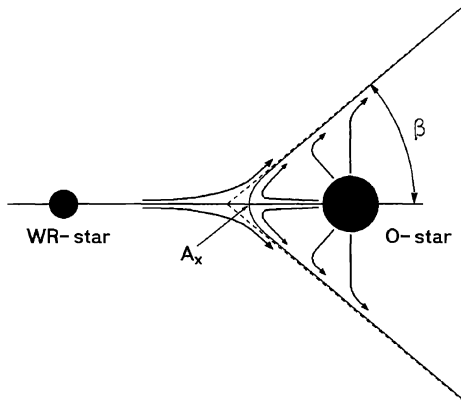


FIG. 4—Illustration of the schematic model for the stationary case.

together with the fitted curves from the corresponding model functions. It will then become apparent that the adopted long period leads to considerably less scatter in the data than the short period.

5. COLLIDING WIND MODEL FOR A WOLF-RAYET – O STAR SYSTEM

5.1 The Model

A numerical hydrodynamic model, such as presented by Stevens et al. (1992) and applied to the WR stars V444 Cyg and WR 140, is well suited to describe the physical nature of the emission peaks in WR 79. In the following, it is shown that a simple geometrical model already suffices to model the emission peaks and their observed periodic motions on the flat-topped C III line and to derive quantitative results which can be compared to the observations.

The binary model discussed in the following consists of an O star primary and a WC star secondary with the following assumed properties: Both have mass loss due to high-velocity radially symmetric stellar winds. The mass-loss rate of the WR star is several times larger than that of the O star. Abbott et al. (1986) derived for WR 79 $\dot{M}_{\text{WR}} = 5 \times 10^{-5} M_{\odot} \text{yr}^{-1}$ from radio astronomical observations, and $v_{\text{WR},\infty} = 3300 \text{ km s}^{-1}$ from UV spectroscopy. These numbers were revised to $\dot{M}_{\text{WR}} = 9 \times 10^{-5} M_{\odot} \text{yr}^{-1}$ and $v_{\text{WR},\infty} = 2270 \text{ km s}^{-1}$ by Willis (1991). For O5–O7 V stars, Lamers and Leitherer (1993) derived $\dot{M}_{\text{O}} = (1.7 \dots 0.5) \times 10^{-6} M_{\odot} \text{yr}^{-1}$ and $v_{\text{O},\infty} = (2900 \dots 2300) \text{ km s}^{-1}$. These data are used in a preliminary calculation for the boundary curve of the interacting winds, assuming the winds to have reached their terminal velocities prior to collision.

The “wind cone” with a half-opening angle β is formed by the perpendicular components of the winds where they meet at equal dynamical pressures,

$$\rho_{\text{WR}} v_{\text{WR}}^2 = \rho_{\text{O}} v_{\text{O}}^2, \quad (1)$$

(see Fig. 4). The apex A_x of the cone, i.e., the stagnation point of the winds, is located on the line which connects the centers of the two stars. The separation between the stellar

centers is a , the distances from the centers to A_x are $r_{\text{WR},X}$ and $r_{\text{O},X}$, respectively:

$$a = r_{\text{WR},X} + r_{\text{O},X} \quad (2)$$

(see also Lührs 1991, Stevens et al. 1992).

With

$$Q = \frac{\dot{M}_{\text{O}} v_{\text{O}}}{\dot{M}_{\text{WR}} v_{\text{WR}}}, \quad (3)$$

a quadratic equation is obtained. The solution for $r_{\text{O},X} < a$ is

$$\frac{r_{\text{O},X}}{a} = \frac{\sqrt{Q} - Q}{1 - Q} = \frac{\sqrt{Q}}{1 + \sqrt{Q}}, \quad (4)$$

as already shown by Huang and Weigert (1982), together with the boundary curves between the interacting stellar winds as a function of Q . Details are given in Lührs (1991).

6. RADIATION FROM THE COLLIDING WIND REGION

6.1 Source of the Additional C III Emissions

To a first approximation, the O star and its spherically outflowing wind constitute an obstacle in the path of the supersonic wind of the WR star, leading to the formation of a bow shock. Assuming a fully ionized gas, the temperature T behind the impact zone is

$$T = \frac{1}{\mathfrak{R}} \frac{3}{16} u^2, \quad (5)$$

with $\mathfrak{R} = 1.403 \times 10^4 \text{ J kg}^{-1} \text{ K}^{-1}$ for the mixture of 75% H and 25% He in mass (yielding upper limits for the cooling times discussed below) and u the velocity component perpendicular to the shock front, created by the interaction of the two winds. According to Eq. (5), the collision of the WR wind with the O-star wind heats the gas in the vertex region to temperatures of the order 10^7 K .

The different conditions for the C III emission are illustrated for three zones:

(1) Near the vertex of the cone and in the vicinity of the O star, the temperatures due to the wind collision are above 10^7 K . The heating by the O6 star also leads to higher ionization stages than C III.

(2) The adjacent region, where the gas is less heated by the O star, and the smaller impact angles of the winds reduce the collisional heating down to the million degree range, the short cooling times support the recombination to C III, see, e.g., Cox and Tucker (1969).

(3) In the outer regions of the wind cone where the temperatures are already low and the impact angles are sufficiently small, C III might be excited.

The quantitative contributions under the different conditions along the wind cone require calculations which are beyond the scope of this observational paper and will be presented in a forthcoming publication. Instead, we shall now concentrate on the geometry of the system.

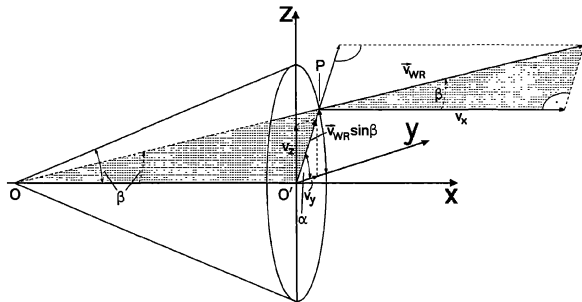


FIG. 5—Components of the wind velocity in the wind cone (see text).

7. REGION OF INTERACTION AS SEEN BY THE OBSERVER

7.1 The Geometrical Model

A simple geometrical model of the WR system is chosen as a substitute for a hydrodynamical model in order to present the different aspects of the wind cone with respect to the observer. The effects of the Coriolis forces are presently neglected and introduced in Sec. 8. In the following, the positions of the two peaks on the flat C III profile are represented by their *maxima*.

Figure 5 shows a circle cutting through the mantle of the wind cone (see Fig. 4) with the half-opening angle β , and defines the components of the wind velocity v_{WR} at point P. The projections onto the line of sight of the observer are illustrated in Fig. 6.

The motion of the WR star around the center of mass of the binary is described by the phase angle φ . At $\varphi=0^\circ$ the WR star has maximum positive radial velocity, at $\varphi=90^\circ$ the WR star is exactly behind the O star. In the latter position

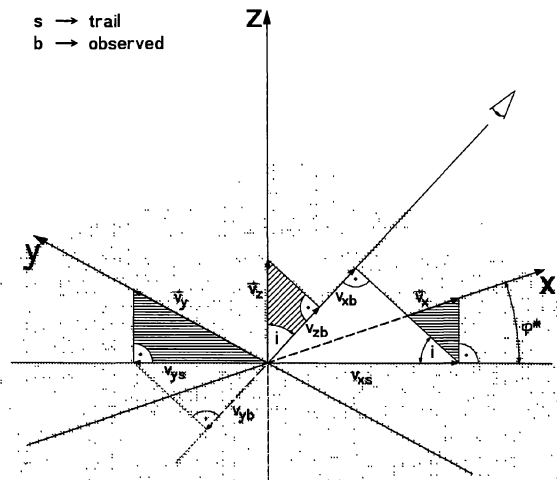


FIG. 6—The origin of the coordinate system, which moves around the center of gravity of the binary, lies in the apex of the comoving cone. The x axis corresponds to the axis of symmetry of the cone. The x, y, z components of the wind velocity in the bow-shock region are projected onto the line of sight of the observer, which is inclined to the z axis by the angle i . v_x and v_y are first projected onto the traces of the components in the x-y plane and then onto the line of sight. The z component is directly projected onto the line of sight.

the opening of the wind cone points towards the observer and the C III peaks are at angle $\varphi^*=0^\circ$ (uncorrected for Coriolis forces, see Fig. 6).

From the components shown in Fig. 5 and Fig. 6, one obtains the wind velocity in the line of sight of the observer

$$v_{\text{obs}} = v_{WR}(-\cos \beta \cos \varphi^* \sin i + \sin \beta \cos \alpha \sin \varphi^* \sin i - \sin \beta \sin \alpha \cos i). \quad (6)$$

With

$$\alpha^* = \arctan \frac{\tan(90^\circ - i)}{\sin \varphi^*}, \quad (7)$$

$$v^* = v_{WR} \sin \beta \sqrt{1 - \sin^2 i \cos^2 \varphi^*}, \quad (8)$$

we finally obtain (see also Neutsch et al. 1979)

$$v_{\text{obs}} = \underbrace{-(v_{WR} \cos \beta \sin i) \cos \varphi^*}_{\text{Term 1}} + \underbrace{v^* \cos(\alpha + \alpha^*)}_{\text{Term 2}}. \quad (9)$$

Keeping the four variables v_{WR} , β , i , and φ^* constant, it is seen that *Term 1* represents a constant mean velocity \bar{v} . Superimposed is *Term 2*. While α varies from 0° to 360° , $\cos(\alpha + \alpha^*)$ assumes all values between $+1$ and -1 . Thus v_{obs} oscillates around *Term 1*, reaching the two extreme radial velocities

$$v_{\text{obs,red}} \equiv v'_{\text{red}} = \text{Term 1} + v^*, \quad (10)$$

$$v_{\text{obs,blue}} \equiv v'_{\text{blue}} = \text{Term 1} - v^*. \quad (11)$$

While the phase angle varies through $0^\circ \leq \varphi^* < 360^\circ$, \bar{v} moves along a cosine curve [see Eq. (9)]. The difference $2v^* = v'_{\text{red}} - v'_{\text{blue}}$ is equal to the width of the *peak profile*.

7.2 Determination of the System Parameters From v^* and \bar{v}

During the orbital cycle, \bar{v} oscillates between the velocities $v_{WR} \cos \beta \sin i$ and $-v_{WR} \cos \beta \sin i$. The half width of the *peak profile* v^* also varies periodically and reaches the extrema

$$v^*_{\text{min}} = v_{WR} \sin \beta \cos i, \quad (12)$$

and

$$v^*_{\text{max}} = v_{WR} \sin \beta. \quad (13)$$

\bar{v} reaches extrema at $\varphi^*=0^\circ$ and $\varphi^*=180^\circ$ (see Fig. 7). For the case of long-period systems where the Coriolis forces can be neglected, we obtain the parameters i , v_{WR} , and β from

$$\cos i = \frac{v^*_{\text{min}}}{v^*_{\text{max}}}, \quad (14)$$

$$v_{WR} = \sqrt{(v^*_{\text{max}})^2 + (v_{WR} \cos \beta)^2}, \quad (15)$$

$$\tan \beta = \frac{v_{WR} \sin \beta}{v_{WR} \cos \beta}. \quad (16)$$

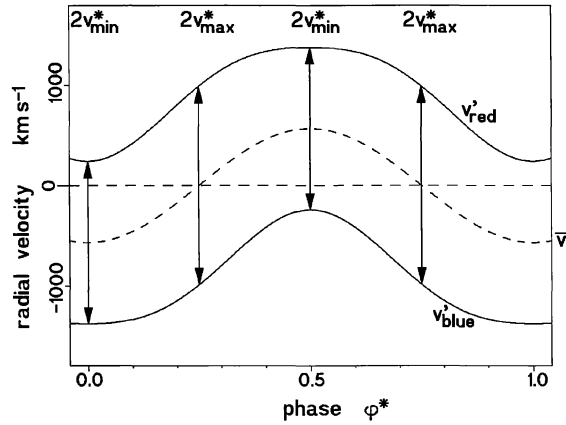


FIG. 7—Radial-velocity curves of the individual peaks on the C III line, v'_{red} , v'_{blue} (solid curves) and the center of gravity of the peak profile \bar{v} (dashed curve) as functions of the phase ϕ^* of the profile peaks, shown for half-opening angle $\beta=45^\circ$, inclination angle of the system $i=35^\circ$, and mean wind velocity $v_{WR}=1400 \text{ km s}^{-1}$. $2v^*_{min}$ and $2v^*_{max}$ are marked by double arrows.

Independent checks of the values v_{WR} and β are given by the relation

$$\bar{v}^2 = v_{WR}^2 \cos^2 \beta - \cot^2 \beta v^{*2}. \quad (17)$$

In the present case, Coriolis forces acting on the wind cone cannot be neglected and are modeled by the angle θ between the axis through the centers of the two stars and the axis of the bow-shock region (see Sec. 7.1), leading to

$$\bar{\varphi}^* = \phi^* - \theta = \phi - 90^\circ - \theta. \quad (18)$$

The angle ϕ^* in Eqs. (6) to (9) is replaced by $\bar{\varphi}^*$.

8. SYSTEM PARAMETERS FROM THE OBSERVED PROFILE PEAKS

The measured radial velocities of the peaks are fitted by the radial-velocity functions v'_{red} and v'_{blue} (see Eqs. 10 and 11) for the two periods obtained in Sec. 3.2 using the simplex algorithm. The fixed orbital parameters (γ , K_2 , t_0) for each of the periods are taken from Table 3. The fits yield the wind velocity v_{WR} , the inclination angle i , the Coriolis angle θ , and the half-opening angle of the wind cone β . The standard deviations of the best fits with the short and the long period are $\sigma=209.0 \text{ km s}^{-1}$ and $\sigma=121.8 \text{ km s}^{-1}$, respectively (see also Fig. 8). The longer period is now adopted. The final system parameters for WR 79 chosen or derived in the present investigation are summarized in Table 5.

9. COMPUTATION OF THE SYNTHETIC PROFILES

In the following, all angles are measured in radians. Equation (9) is rewritten as

$$\frac{v_{obs} - \bar{v}}{v^*} = \cos(\alpha + \alpha^*) = \bar{u}. \quad (19)$$

α is introduced in Sec. 7 and shown in Fig. 5. We obtain

$$d\alpha = \frac{d\bar{u}}{\sqrt{1 - \bar{u}^2}}. \quad (20)$$

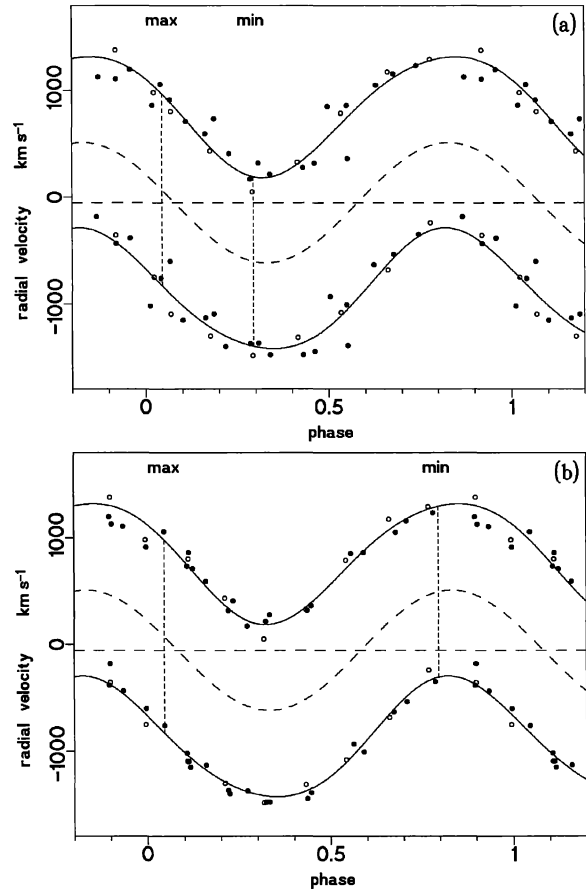


FIG. 8—Radial-velocity data of the peaks on the C III line: (a) fitted by the model obtained with the shorter period, (b) fitted with the longer period; dashed curve: motion of the center of gravity of the peak profile, dashed line: system velocity; small dashed lines mark the maximum and minimum velocity differences.

Because of the rotational symmetry, all sections $d\alpha$ along a given cut, parallel to the base of the cone, are uniformly covered by a luminous fluid. They radiate the C III light

$$I_\alpha d\alpha = \frac{I}{2\pi} d\alpha, \quad (21)$$

which appears as the peak profile.

TABLE 5
Data for WR 79 as Derived in the Present Paper

Name	WR 79, HD 152270
Spectral types	WC7 + O6
Period	$P = (8.89104 \pm 0.00018) \text{ d}$
Inclination angle	$i = 28:0 \pm 1:1$
Velocities	$K_1 = (41.3 \pm 8.6) \text{ km s}^{-1}$ $K_2 = (132.6 \pm 10.8) \text{ km s}^{-1}$ $\gamma = (-55.0 \pm 4.7) \text{ km s}^{-1}$
Masses	$M_{WR} = (11.1 \pm 3.9) M_\odot$ $M_\odot = (35.6 \pm 9.0) M_\odot$
Coriolis angle	$\theta = 16:8 \pm 2:2$
Half opening angle of the cone	$\beta = 39:8 \pm 0:8$
Wind velocity in the cone mantle	$v_{WR} = (1417 \pm 22) \text{ km s}^{-1}$

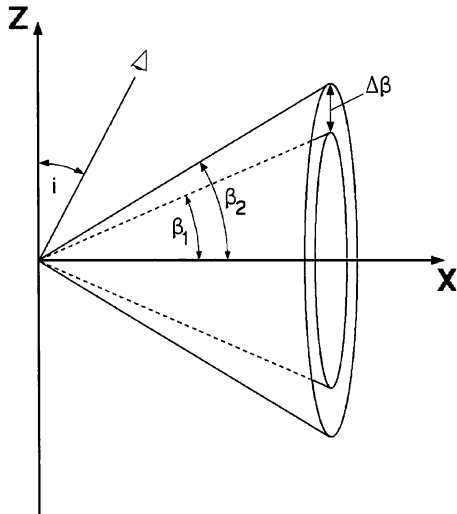


FIG. 9—The cone with a mantle of thickness $\beta_2 - \beta_1 = \Delta\beta$ (thick mantle).

The intensity is unevenly allocated to the different Doppler regions of the peak profile. Since \bar{u} is determined by α , $I_{\bar{u}}$ is given by I_{α} , and $dI_{\bar{u}}$ by dI_{α} . We thus obtain

$$I_{\bar{u}} d\bar{u} = \frac{I}{2\pi} d\alpha = \frac{I}{2\pi} \frac{d\bar{u}}{\sqrt{1-\bar{u}^2}}. \quad (22)$$

The cone, however, does not radiate at the specific angle β only. In a more realistic picture, we assume that a mantle of thickness $\beta_2 - \beta_1 = \Delta\beta$, which will be called the *thick mantle*, is filled with a luminous fluid (Fig. 9). The *peak profile* is obtained by integration over the thick mantle.

At unit distance from the vertex of the cone, the ring area corresponding to a small angle $d\beta$ is $2\pi \sin \beta d\beta$. The distribution function $f(\beta)$ gives the density of the luminous fluid at a given angle β . The total intensity $I(v)$ is given by

$$I(v) dv = \int_{\beta_1}^{\beta_2} 2\pi \sin \beta d\beta I(\beta, v) f(\beta) dv. \quad (23)$$

It is assumed that the luminous fluid declines quadratically to zero density towards the boundaries of the thick mantle according to

$$f(\beta) = \mathcal{E} \times (\cos \beta_1 - \cos \beta)(\cos \beta - \cos \beta_2), \quad (24)$$

where \mathcal{E} is given by

$$2\mathcal{E} = \frac{6}{\pi(\cos \beta_1 - \cos \beta_2)^3}. \quad (25)$$

Along the thick mantle the density is assumed to be constant. In this case the total intensity is given by

$$\begin{aligned} I(v) dv &\equiv I(u) du \\ &= 2\mathcal{E} du \int_{\cos \beta_2}^{\cos \beta_1} \frac{(\cos \beta_1 - \cos \beta)(\cos \beta - \cos \beta_2)}{\sqrt{u^{*2} - (u - \bar{u})^2}} d(\cos \beta), \end{aligned} \quad (26)$$

where u , u^* , and \bar{u} are the velocities v , v^* and \bar{v} normalized to v_{WR} (see Sec. 7.1).

Integration yields

$$I(u) du = \frac{6}{\pi(\cos \beta_1 - \cos \beta_2)^3} \{J(u)\} du, \quad (27)$$

where

$$J(u) = \left\{ \begin{array}{l} [(u \sin j - \cos \beta_2)(\cos \beta_1 - u \sin j) \\ - 0.5(1 - u^2) \cos^2 j](\psi_1 - \psi_2) \\ - [(\cos \beta_1 + \cos \beta_2 \\ - 2u \sin j) \sqrt{(1 - u^2) \cos^2 j}](\cos \psi_1 - \cos \psi_2) \\ + 0.25(1 - u^2) \cos^2 j (\sin(2\psi_1) - \sin(2\psi_2)) \end{array} \right\},$$

with

$$\psi_1 = \arcsin y_1(\cos \beta_1, u),$$

$$\psi_2 = \arcsin y_2(\cos \beta_2, u),$$

$$\sin j = -\sin i \cos \varphi^*,$$

$$\cos j = \sqrt{1 - \sin^2 i \cos^2 \varphi^*},$$

$$y_1 = \min \left[+1, \frac{\cos \beta_1 - u \sin j}{\sqrt{(1 - u^2) \cos^2 j}} \right],$$

$$y_2 = \max \left[-1, \frac{\cos \beta_2 - u \sin j}{\sqrt{(1 - u^2) \cos^2 j}} \right].$$

In Fig. 10 we present a sequence of synthetic *peak profiles* for normalized radial velocities u and phase angles φ^* over one cycle. In the following section the computed profiles are fitted to the corresponding observed profiles.

10. THE MODEL FITTED TO THE OBSERVATIONS

10.1 Synthetic Peak Profiles

So far, the synthetic line profiles are computed in radial-velocity space; for comparison with the measured profiles they are transformed into wavelength space. For matching the observed profiles, the synthetic *peak profiles* are oriented along a parallel to the underlying continuum. Fixed parameters are the inclination angle i and the approximation for the Coriolis forces θ , given in Table 5. The corrected orbital

phase is $\varphi - \theta$. The fitted parameters β_1 and β_2 are optimized for each observed *peak profile*. The results are shown in Fig. 11.

From the respective best-fits, we conclude that the extent $\Delta\beta$ of the mantle at different phases varies between $\Delta\beta = 37^\circ 0$ and $54^\circ 6$, with a mean value of $44^\circ 4 \pm 5^\circ 7$. It remains to be tested whether these variations are caused by real fluctuations.

10.2 Results

Deviations between the observed and the synthetic profiles pertain mostly to the *peak heights* while the *peak widths* match well. Until a more detailed model and/or more observations are available, we suggest that the deviations might be due to clumpiness in the line-forming region. It should be noticed, however, that such deviations from the basic model may last over many cycles (see Fig. 1) and could indicate tertiary effects in the system, to be explained by more observations during different cycles.

(a) The deviations in *relative widths* of the profile peaks are small and can be explained by minor additional emissions.

(b) The deviations of the *profile positions* on the underlying C III line are small.

(c) The largest deviations occur in the *heights of the profile peaks*.

The model used here is based on the simple geometry of the two interacting winds in the binary system, while the physics

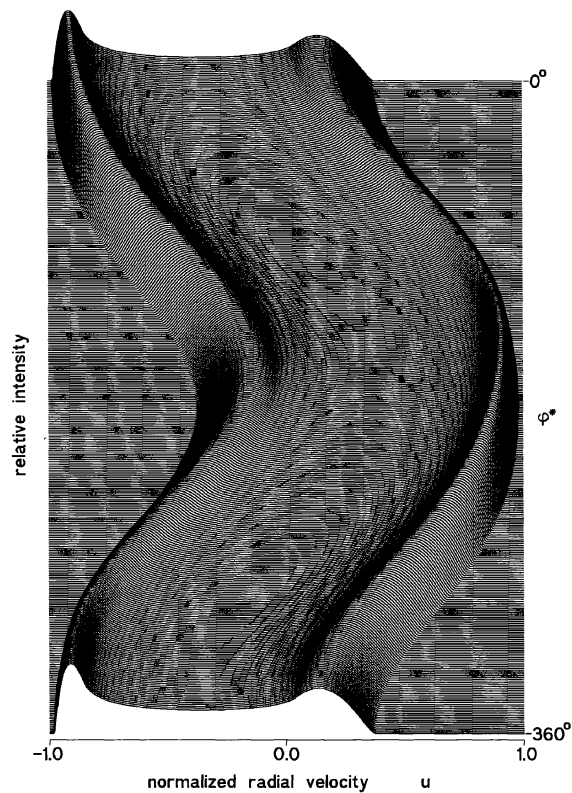


FIG. 10—Synthetic *peak profiles* as functions of the normalized radial velocity u and the phase angle φ^* .

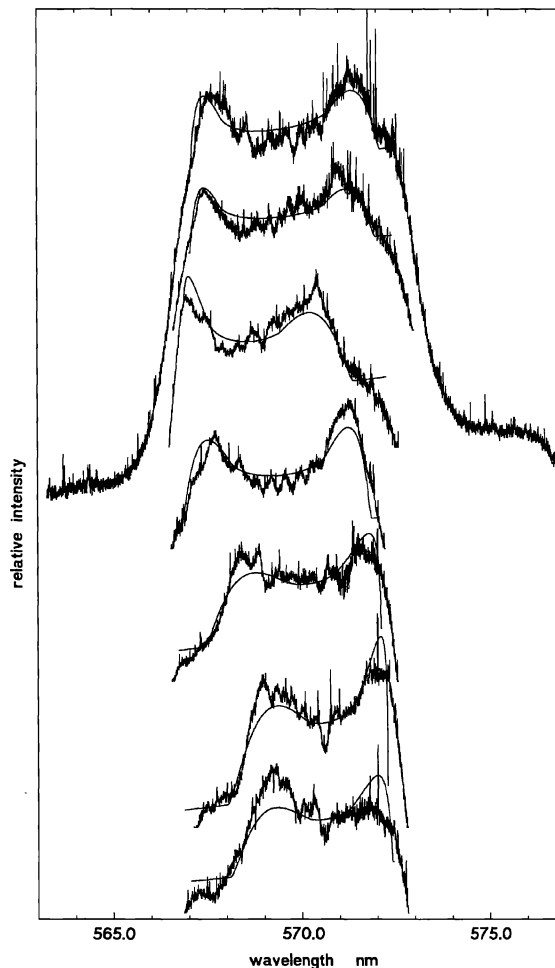


FIG. 11—Fit of the synthetic profiles to the observations. From top to bottom: (a) Corrected phase: $\varphi - \theta = 0.063 \pm 23^\circ$. Fit parameters: $\beta_1 = 32^\circ 9$, $\beta_2 = 72^\circ 5$. The widths of the two observed peaks are reproduced by the synthetic profile; the red peak is broader than the blue one. (b) Corrected phase: $\varphi - \theta = 0.073 \pm 26^\circ$. Fit parameters: $\beta_1 = 32^\circ 1$, $\beta_2 = 69^\circ 1$. The line widths and the height of the blue peak are well reproduced. (c) Corrected phase: $\varphi - \theta = 0.182 \pm 66^\circ$. Fit parameters: $\beta_1 = 23^\circ 1$, $\beta_2 = 67^\circ 9$. The line widths of the two peaks are well reproduced; the heights deviate noticeably. (d) Corrected phase: $\varphi - \theta = 0.512 \pm 184^\circ$. Fit parameters: $\beta_1 = 28^\circ 3$, $\beta_2 = 70^\circ 1$. In this case the two peaks have nearly equal width; deviations are mostly due to different heights. (e) Corrected phase: $\varphi - \theta = 0.629 \pm 226^\circ$. Fit parameters: $\beta_1 = 13^\circ 6$, $\beta_2 = 68^\circ 0$. The widths of the computed peaks deviate noticeably from the observed ones. (f) Corrected phase: $\varphi - \theta = 0.738 \pm 266^\circ$. Fit parameters: $\beta_1 = 16^\circ 5$, $\beta_2 = 63^\circ 3$. Here the narrow and broad line widths have exchanged their positions. This is well modeled by the synthetic curve. (g) Corrected phase: $\varphi - \theta = 0.854 \pm 307^\circ$. Fit parameters: $\beta_1 = 13^\circ 4$, $\beta_2 = 59^\circ 7$. The *line profile* is heavily disturbed, especially concerning the peak heights. As shown in Fig. 1, this disturbance exists over more than 160 periods, suggesting that certain conditions of clumpiness have a very long lifetime.

of the winds is neglected. As has been suggested previously (e.g., Carlberg 1980), radiation-powered winds break up into clumps or slabs of the order of solar radii and more, which lead to inhomogeneous flows. This has been observed in a single WR star (Moffat et al. 1994) and may account for the larger deviations from the simple model discussed here. The effects of small additional emissions and noise are shown below.

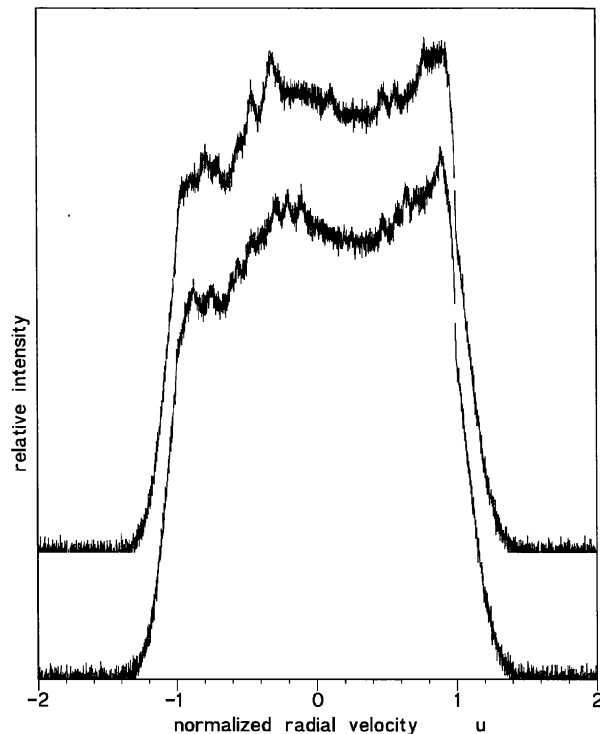


FIG. 12—Superimposed on two equal flat profiles is the synthetic peak profile which corresponds to the corrected phase angle 226° . Besides noise, small emission peaks are added whose total light equals typical observed peaks and which are distributed by a Monte Carlo method. Only the arbitrarily chosen starting points for the random number generator are different for the two profiles shown here.

11. SIMULATIONS OF THE C III LINE

The simulation parameters are derived from the observed spectra. The overlying small spectral features are modeled using Monte-Carlo simulations.

The C III line is represented by a rectangular base with Gaussian wings on either side and a synthetic *peak profile* on the flat top. With Monte-Carlo simulations, different sets of minor structures, modeled after those found in the observations, are distributed over a given basic peak profile. Using the synthetic profiles at the corrected phase angle 226° , the results from two different runs are shown in Fig. 12. The additional small emissions modify the peak profile in a way similar to the observed profiles, e.g., the observed flattened red peak is well simulated when using one starting point, while another one leaves the same peak undisturbed.

12. SUMMARY AND CONCLUSIONS

From the data presented here and in earlier investigations, the orbital parameters for the binary system WR 79 are determined: period P , inclination angle i , maximum orbital velocities K_1 for the primary (O star) and K_2 for the secondary WR star, γ velocity of the system, masses of the two components M_{WR} and M_O , half-opening angle β of the interacting wind cone, and mean wind velocity v_{WR} in the cone (see Table 5).

Over the orbital cycle, the C III line of WR 79 shows, on its flat top, always two noticeable peaks of varying shape and changing position. The radial velocities of the peaks permit an independent determination of the inclination angle i by a global solution of the RV curves of the peaks.

In WR 79, the Wolf-Rayet wind is considerably denser and faster than the wind of the O star. In the proposed model it is thus assumed that the O star and its wind are embedded in the wind of the WR star. The boundary surface is conelike and rotationally symmetric with respect to the line connecting the two stars. The shape is given by the ratio $Q = \dot{M}_O v_O \dot{M}_{WR}^{-1} v_{WR}^{-1}$, the aspect for the observer is modified by the Coriolis force.

Our derived value of β corresponds to a Q value of 0.02 (see, e.g., Huang and Weigert 1982). Using Willis' (1991) values for the mass loss and terminal wind velocity of the WR star in WR 79, this Q value is compatible with the mass-loss rate of $1.6 \times 10^{-6} M_\odot \text{ yr}^{-1}$, and the wind velocity of 2500 km s^{-1} of the O star. Interpolation of the mass-loss rates of single stars of types O5V and O7V, given by Lamers and Leitherer (1993), yields $\dot{M}_O = 10^{-6} M_\odot \text{ yr}^{-1}$ and $v_O = 2500 \text{ km s}^{-1}$, in good agreement with the estimate obtained here.

Since the flat-topped C III line is not blended with lines of other ions, we are able to observe and analyze the superimposed varying emission peaks which suggest the presence of an extended cone-shaped bow-shock region, created by the colliding stellar winds around the O star. The short cooling times of the gases, heated to X-ray temperatures at the vertex of the cone, and the increasingly lower temperatures along the cone due to more grazing collisions, suggest a large region where C III emission is produced. This agrees well with the behavior of the observed C III subpectrum.

Geometrical analysis of the orbital aspects of the bow-shock region leads to functions for the radial velocities of the two emission peaks. WR stars of subclasses WC 5 to WC 8 where the C III 569.59 nm line shows a broad flat-topped profile and superimposed smaller structures may be studied by the methods introduced in the present paper.

Theoretical peak profiles derived from the colliding wind model and the basic parameters of the system show good agreement with the varying shapes of the observed peak profile on the flat-topped C III line. Minor deviations from the expected shapes can be modeled by Monte-Carlo simulations and may be due to clumping of the gas. Several observed long-lasting secondary structures suggest streams of a considerable lifetime. Since the colliding wind model was introduced for WR 79, it has been applied to at least one other system, B22 in the Large Magellanic Cloud (Bartzakos et al. 1995).

Sincere thanks go to Waltraut Seitter for suggesting this investigation and for extensive discussions and support, to Hilmar Duerbeck for providing the 1988 and 1989 data and continued help in solving scientific as well as technical problems, to Rudolf Duemmler and Peter Schuecker for computer programs and advice, to Michael Nolte for untiring services during all phases of this investigation. I am grateful to Anthony Moffat for fruitful discussions. The competent and

friendly assistance of the staff at the European Southern Observatory, La Silla, is gratefully acknowledged. This paper is based on a Ph.D. thesis by the author.

REFERENCES

- Abbott, D. C., Biegging, J. H., Churchwell, E., and Torres, A. V. 1986, *ApJ*, 303, 239
- Bartzakos, P., Moffat, A. F. J., and Niemela, V. S. 1995, in Proc. IAU Symp. 163, *Wolf-Rayet Stars: Binaries, Colliding Winds, Evolution*, ed. K.A. van der Hucht and P. M. Williams (Dordrecht, Kluwer), p. 406
- Caceci, M. S., and Cacheris, W. P. 1984, *BYTE*, 9, 340
- Carlberg, R. G. 1980, *ApJ*, 241, 1131
- Cox, D. P., and Tucker, W. H. 1969, *ApJ*, 157, 1157
- Duerbeck, H. W., Seitter, W. C., and Duemmler, R. 1987, *MNRAS*, 229, 653
- Hoffmeister, C., Richter, G., and Wenzel, W. 1990, *Veränderliche Sterne* (Leipzig, Johann Ambrosius Barth), p. 283
- Huang, R. Q. and Weigert, A. 1982, *A&A*, 112, 281
- Lamers, H. J. G. L. M., and Leitherer, C. 1993, *ApJ*, 412, 771
- Lührs, S. 1991, Ph.D. Thesis, Astronomical Institute, University of Münster
- Moffat, A. F. J., Lépine, S., Henriksen, R. N., and Robert, C. 1994, *Ap&SS*, 216, 55
- Neutsch, W., Schmidt, H., and Seggewiss, W. 1979, *Veröffentl. Astron. Inst. Bonn No. 92*
- Neutsch, W. 1979, *Veröffentl. Astron. Inst. Bonn No. 93*
- Neutsch, W., Schmidt, H., and Seggewiss, W. 1981, *AcA*, 31, 197
- Pollock, A. M. T., Haberl, F., and Corcoran, M. F. 1995, in Proc. IAU Symp. 163, *Wolf-Rayet Stars: Binaries, Colliding Winds, Evolution*, ed. K.A. van der Hucht and P. M. Williams (Dordrecht, Kluwer), p. 512
- Seggewiss, W. 1974, *A&A*, 31, 211
- Smith, L. F., Shara, M. M., and Moffat, A. F. J. 1990, *ApJ*, 358, 229
- St.-Louis, N., Drissen, L., Moffat, A. F. J., and Bastien, P. 1987, *ApJ*, 322, 870
- Stevens, I. R., Blondin, J. M., and Pollock, A. M. T. 1992, *ApJ*, 386, 265
- Struve, O. 1944, *ApJ*, 100, and 189, 384
- van der Hucht, K. A., Hidayat, B., Admiranto, A. G., Supelli, K. R., and Doom, C. 1988, *A&A*, 199, 217
- Willis, A. J. 1991, in Proc. IAU Symp. 143, *Wolf-Rayet Stars: and Interrelations with Other Massive Stars in Galaxies*, ed. K.A. van der Hucht and B. Hidayat (Dordrecht, Kluwer), p. 265